NANO LETTERS

pubs.acs.org/NanoLett

Fabrication and Microstructure Control of Nanoscale Mechanical Testing Specimens via Electron Beam Lithography and Electroplating

Michael J. Burek,[†] and Julia R. Greer*,[‡]

[†]University of Waterloo, Waterloo, ON N2L 3G1, Canada, and [‡]Division of Engineering and Applied Science, California Institute of Technology, Pasadena, California 91125

ABSTRACT It has been demonstrated that the mechanical properties of materials change significantly when external dimensions are confined to the nanoscale. Currently, the dominant fabrication method for mechanical testing specimens with nanometer dimensions is by using focused ion beam (FIB) milling, which results in inevitable Ga^+ induced damage to the microstructure. Here, we report a FIB-less fabrication technique to create arrays of vertically oriented gold and copper nanopillars based on patterning polymethylmethacrylate by electron beam lithography and subsequent electroplating into the prescribed template. This fabrication process is capable of producing a wide range of microstructures: from single crystals and nanotwinned, to bi-, poly-, and nanocrystalline mechanical testing specimens with diameters from 750 down to 25 nm with the diameter range below 100 nm previously inaccessible by FIB.

Over the past decade, the nanomechanics community has renewed its interest in the investigations of size-dependent mechanical properties due to the advancements in the instrumental resolution and in computational capabilities. In the case of single crystalline metals, the size effects manifest themselves as a pronounced increase in compressive strength when the external dimensions are reduced to the micrometer and submicrometer scale.[1−14] To study the size-dependent material strengths, cylindrical pillars with diameters ranging from several micrometers down to several hundred nanometers are fabricated by utilizing a focused ion beam (FIB) milling method for subsequent uniaxial compression testing. This approach was first introduced by Uchic et al.[1,15] and later extended by Greer et al.[2] and others for uniaxial compression tests of single-crystalline pillars with submicrometer diameters. Although most research groups report a pronounced power-law relationship between the attained strength and pillar diameter,[16] there remains contention as to the influence of Ga^+ induced damage on the nanopillar strength and commencing plastic deformation mechanism.[15,17] Furthermore, nanopillars prepared by the top-down FIB milling process have a noticeable vertical taper, which becomes more severe as the pillar diameter is reduced, and thus results in the undesirable nonuniform strain distribution within the pillar.[18] One research group has successfully manufactured Mo micropillars from a eutectic alloy of Mo−Ni_3Al with subsequent etching of the sacrificial Ni_3Al phase, and unlike all the groups who fabricate their pillars by using the FIB their samples do not exhibit any size dependence and attain nearly theoretical strength values for all diameters.[19,20] Unlike the FIB-manufactured pillars, whose initial dislocation densities are on the order of 10^{12} m^{-2}, these pillars are pristine, that is, defect-free, thereby rendering the attainment of nearly theoretical strengths not surprising. These findings suggest that the use of Ga^+ ions during the fabrication process may significantly affect the observed deformation behavior. While the origins of the very high strengths attained by crystals at the nanoscale are still being debated, many agree with the presence of a pronounced size effect. To probe deformation mechanisms and microscopic stress−strain response without the additional complexity of ion effects, there is desperate need to develop FIB-less fabrication methods resulting in nonzero initial dislocation density structures for nanoscale mechanical testing.

Herein, we report a fabrication procedure that does not utilize FIB milling to create isolated, vertically oriented, and virtually taper-free metallic nanoscale mechanical testing specimens with diameters from 750 down to 25 nm. This fabrication method also allows control over the pillar microstructure from nanocrystalline to single-crystalline. Our fabrication method involves lithographic patterning of polymethylmethacrylate (PMMA) resist with electron beam lithography, followed by metal electrochemical deposition into the prescribed resist template. Fundamentally, this fabrication approach is analogous to other template-based syntheses wherein one-dimensional nanostructures are fabricated by electroplating into the pores of either polycarbonate or alumina membranes.[21−26] Although template-based synthesis has been extensively studied, it has not been applied to the fabrication of nanomechanical testing specimens. The primary reason for this is the limited control over pore size and placement in conventional porous membranes. To combat this limitation, we have employed a lithographic method for template fabrication that allows full and independent control over pore size and spacing. To the

Received for review: 09/1/2009
Published on Web 00/00/0000

DOI: 10.1021/nl902872w | *Nano Lett.* **XXXX,** *xxx,* 000-000

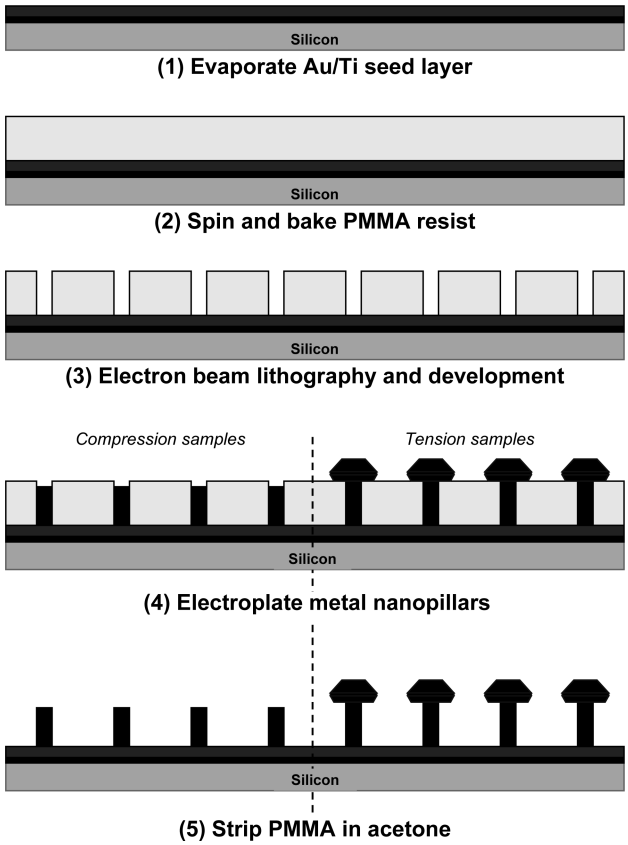

FIGURE 1. Schematic representation of the FIB-less fabrication steps for compression and tension mechanical testing specimens.

best of our knowledge, this is the first report on the development of a nondamaging technique to create isolated metal nanopillars for compression and tensile mechanical tests with sub-100 nm diameters and with nonzero initial dislocation densities, that is, dissimilar to nanowhiskers.[27] Also discussed in this report is a novel sacrificial metal masking sample preparation method for transmission electron microscopy (TEM) analysis of these nanopillars.

Our technique has several major advantages over the conventional FIB milling of nanopillars. First, by replacing FIB fabrication with a procedure that does not utilize ion bombardment, the metallic nanopillar crystalline structure is absent of Ga^+ ion damage. Second, by using electron beam lithography, pillars with diameters much smaller than those possible with the FIB technique can be readily fabricated. Third, when optimized this fabrication method greatly reduces pillar tapering relative to FIB fabrication and virtually eliminates the presence of any appreciable strain-gradients in the deformation process. Finally, the FIB fabrication process is inherently slow and significantly limits the sample throughput time. The proposed fabrication method has a much higher throughput with hundreds of pillars fabricated simultaneously on the same substrate.

Figure 1 shows a schematic illustration of our fabrication process for the creation of compressive and tensile mechanical testing specimens. In this work, Au and Cu nanopillars

TABLE 1. Polymethylmethacrylate (PMMA) Resist and Electron Beam Exposure Parameters for Nanopillar Samples of Various Diameters Intended for Compression Testing[a]

pillar dimensions		resist parameters		exposure parameters
d (nm)	L (nm)	dilution (%)	speed (rpm)	dose (μC/cm^2)
25	100	4	2500	2600
50	200	4	2500	1600
100	400	7	3000	1450
150	600	7	1500	1600
200	800	9	4500	1550
250	1000	9	2000	1500
500	2000	11	2500	1600
750	3000	11	1500	1750

[a] The resist type is 950 kD PMMA diluted in anisole (MicroChem Corp.). The electron doses were observed for a pattern density of 1.0×10^6 cm^{-2}.

were intentionally chosen to demonstrate the feasibility of the process; however the technique is not limited to these particular metals and can be applied to a wide variety of electroplatable systems. Nanopillar arrays were fabricated on Si substrates ranging in size from ~1 cm^2 chips to 100 mm diameter wafers. Prior to applying the PMMA resist, a 20 nm thick Ti adhesion layer and a 100 nm thick Au seed layer were deposited on the substrate by electron beam evaporation. This conductive seed layer acts as a cathode in the subsequent electroplating steps. The choice of metal and the thickness of this conductive layer are noncritical, but need to be appropriate for the electrochemical processing, that is, the film does not form an oxide, and for the nanomechanical testing, that is, strong adhesion between the film and the Si substrate. The substrates were spin coated with various dilutions of 950 kD PMMA in anisole (MicroChem Corp.). Table 1 outlines the PMMA resist conditions used to generate the specific range of desired pillar diameters. Generally, pillars meant for compression testing are required to have an aspect ratio of at least 1:3 (height/diameter) and no greater than 1:6. This ensures that nanopillars are tall enough to experience homogeneous deformation without significant effects of top and bottom constraints, but not so tall as to buckle during compression testing. An aspect ratio of ~1:4 was selected as the standard for the nanopillars fabricated in this report. Even though the nanopillar aspect ratio is ultimately governed by plating time, it is imperative that the PMMA resist thickness closely matches the intended nanopillar height. This requirement is critical for the fabrication of taper-free pillars with sub-100 nm diameters and also eliminates the use of excessive electron doses. The resist dilutions were selected such that the spin conditions were maintained between 1500 and 4500 rpm, thus ensuring uniform PMMA films. Following spin coating, the PMMA layer was baked at 180 °C for 15 min. The resist was then exposed using a Leica EBPG5000+ electron beam lithography system operating at an acceleration voltage of 100 kV. For all exposures, the beam current was maintained between 650 and 800 pA and the beam step size was 5 nm. The resolution of electron beam lithography is primarily a function of the electron dosage, whose optimal value de-

DOI: 10.1021/nl902872w | *Nano Lett.* **XXXX,** *xxx,* 000-000

pends on the resist type and thickness, minimum feature size, and pattern density. Since these relations are inherently nonlinear, a dose matrix was routinely used in order to empirically determine the optimal exposure conditions. Table 1 also provides the optimal electron doses for the corresponding PMMA resist parameters. Exposure patterns were computer generated and are extremely flexible, allowing for precise isolation of nanopillars and simultaneous fabrication of the indicator markers, as the individual nanopillars were routinely spaced up to 50 μm apart. Immediately following exposure, the PMMA was developed for 60 s in a 1:3 solution of methylisobutylketone (MIBK) and isopropyl alcohol (IPA) followed by a 5 s rinse in IPA.

Following development of the PMMA, the resist template was ready for metal electroplating. Electroplating was performed using a two electrode configuration in a 1.0 L glass beaker. The Au seed layer underneath the resist template acted as the cathode, and a Pt-coated Ti mesh was used as an insoluble anode. The Au plating solution used was a commercially available, ready to use $[Au(SO_3)_2]^{2-}$ plating bath (Technic Gold 25-ES, Technic, Inc.). The Cu plating solution was made in house using 125 g/L $Cu(SO_4) \cdot 5H_2O$ and a supporting electrolyte of 50 g/L H_2SO_4. The homemade Cu plating solution was mixed with deionized water and reagent grade chemicals. The bath temperature was maintained at 60 °C in the case of Au deposition and at room temperature for Cu deposition. The plating solution was mechanically stirred and electroplating was performed under both galvanostatic (DC) and reverse pulse (AC) conditions. In DC plating, the current densities were varied between 2.5 to 10 mA/cm^2 for Au electroplating and between 10 to 35 mA/cm^2 for Cu electroplating. For AC plating, the cathodic/anodic current ratio was varied between 5:1 and 1:1, and in all cases the cathodic pulse was held for 5 s followed by the anodic pulse for 1 s. The electroplating rate was estimated using Faraday's law, and deposition was stopped when the desired pillar height was achieved. Occasionally, fresh electrolytes were used, but in most cases the solutions were preconditioned electrolytes reused from earlier experiments. Following metal deposition, the PMMA resist was stripped in a bath of acetone at room temperature and rinsed in acetone and IPA. In the case of pillars to be used for tension tests, metal was intentionally overplated for a brief period to form a cap on the top of the pillar. Following removal of the resist template, these caps remain and can be accessed by a set of microgrips in order to tense the pillar.

The nanopillars were characterized by scanning electron microscopy (SEM), FIB imaging, and transmission electron microscopy and small-area electron diffraction (TEM and SAED, FEI Tecnai F20). SEM provided immediate confirmation of nanopillar geometry to validate the lithographic parameters, while FIB imaging was employed as a primarily qualitative judgment of nanopillar microstructure. FIB imaging is capable of revealing grain and twin boundary contrast,[28,29] thus providing rapid feedback to adjust electroplating parameters to achieve the desired pillar microstructure. Specifically, FIB imaging was extremely useful for determining the electroplating parameters that yielded single-crystal microstructures in copper nanopillars. All FIB images were generated with a 30 kV Ga^+ beam with a current of ~50 pA. As an inherently destructive method, FIB imaging is not available as a technique prior to nanomechanical testing. However, the speed of this technique allowed for imaging hundreds of pillars in order to infer the percentage of pillars with acceptable microstructures given a specific set of electroplating parameters. Because of the resolution limitations and the destructive nature of the technique,[28,29] FIB imaging was limited to pillars with a minimum grain size of ~50 nm (for Cu) and minimum pillar diameter of ~200 nm.

To validate the nanopillar microstructure, TEM and SAED were utilized on a select number of representative pillars. Two sample preparation schemes were used to generate samples for TEM and SAED analysis. The first sample preparation scheme was via the "conventional" lamella lift out[29] and its subsequent placement onto a Cu TEM grid with a micromanipulator (AutoProbe 200, Omniprobe, Inc.). Following removal of the PMMA, nanopillars intended for TEM analysis were identified by SEM in an SEM/FIB dual beam system (Nova NanoLab 600, FEI Company) and then coated in a several micrometer thick layer of Pt by local chemical vapor deposition (CVD) via gas injection system. The Pt is deposited through the decomposition of a Pt-based organometallic compound using the localized raster of either the electron or ion beam. As a result however, the final Pt is not pure and contains a significant fraction of carbon. Coating the pillars in Pt is necessary to protect against the redeposition and ion damage during the lift out process. Following Pt deposition, a 30 μm long by 5 μm wide by 5 μm deep lamella was milled around the pillar in order to isolate it. The lamella was then lifted out via micromanipulator and attached with Pt to a standard four post Cu TEM lift out grid. The Pt coating was then carefully thinned from both sides using a 30 kV ion beam operating at ~10 pA current to a final thickness of ~100 nm, after which the pillar was ready for TEM analysis.

This method is relatively quick with a high yield, and is most appropriate for larger pillars, which are not electron transparent. However, the final FIB thinning step significantly limits application of this method. First, FIB thinning (especially at high acceleration voltages) creates irreversible damage to the sample and has also been known to induce recrystallization of fine grain morphologies.[30] This eliminates the possibility of performing microstructural analysis such as high resolution imaging, dislocation density determination, and grain size. As such, this technique does not satisfy the major requirements of the nanomechanical community. Since the nanopillar fabrication method is capable of producing pillar diameters, much smaller than the elec-

DOI: 10.1021/nl902872w | *Nano Lett.* **XXXX,** *xxx,* 000-000

tron transparent limit for most metals, a second sample preparation technique, which does not involve FIB thinning, was developed.

The second sample preparation scheme was a novel sacrificial metal masking method whereby following PMMA removal the entire pillar array was coated in ~500 nm of Cr via sputter deposition. The Cr layer served as the sacrificial masking layer. Nanopillars intended for TEM analysis were again identified via SEM and then isolated by FIB by milling 30 μm long by 5 μm wide by 5 μm deep lamella. This was followed by lift out and placement on to a Cu TEM grid via micromanipulator. With a thick Cr barrier, any exposure of the ion beam to the chromium-coated pillars during the milling and lift out process was not able to reach the pillars. However, redeposition of milled material on the Cr-coated pillars was inevitable, hence the need for a masking layer. Following attachment of the lamella to the TEM foil, the Cr layer was etched away using a selective Cr etchant (3.0% $KMnO_4$ + 0.5% NaOH + H_2O, CR-100 recipe by Cyantek, Inc.). In most cases, the sodium hydroxide concentration in the commercial etchant recipe was increased to improve the etch speed. This etching step left pillars ready for TEM and SAED analysis and free of any ion damage and redeposition. A major advantage offered by this method is that it enables nanomechanical testing of the nanopillars directly on the TEM grid. As such, it is possible to investigate the evolution of deformation in the same pillar by doing, for example, in situ TEM analysis or ex situ imaging before and after compression. Despite the advantage of this sample preparation scheme, the entire process is inherently slow with a low yield. As such, more work is currently being done to improve the throughput of this technique.

Figure 2a–h shows representative images of Au nanopillars prepared for compression tests electroplated at 3.5 mA/cm^2. The FIB-less process has clear advantage over the conventional FIB fabrication with respect to lower limit of sample size and nanopillar tapering. As a point of comparison, Figure 2i shows a Au nanopillar with diameter of ~300 nm prepared by conventional FIB milling methodology,[2,15] clearly demonstrating a more pronounced taper compared with pillars produced by the FIB-less technique. The electron beam lithography process was well optimized and nanopillars with 25 nm diameters were readily achieved. Not only is the FIB-less process absent of any Ga^+-induced damage, but nanopillar tapering is virtually nonexistent and the samples are even closer to being strain-gradient free during testing. Nanopillars fabricated with under or over exposed PMMA resist suffered from significant nanopillar tapering (results not shown). In larger diameter pillars, under exposing the resist resulted in a negative taper angle and mechanically unstable pillars, while in smaller diameter pillars under exposure resulted in missing pillars. For all pillar sizes, over exposure either led to nanopillars with larger than intended diameters and, in the case of significant over exposure, led to a positive taper.

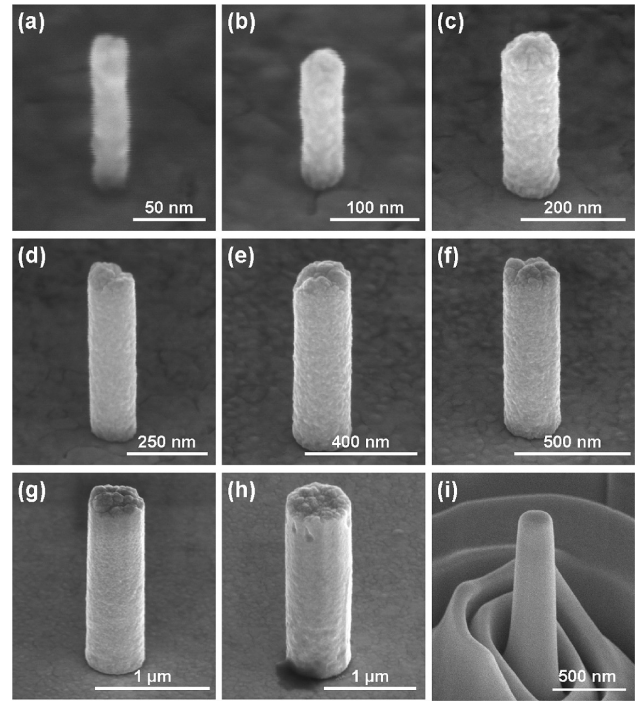

FIGURE 2. SEM images of Au nanopillars prepared for compression tests with diameters of 25, 50, 100, 150, 200, 250, 500, and 750 nm (a–h). All nanopillars were fabricated with an aspect ratio of ~1:4 with the exception of the 25 nm diameter pillar that has an aspect ratio of ~1:8. A SEM image of a gold pillar with a nominal diameter of ~300 nm prepared by FIB milling is shown in (i). A clear reduction in pillar tapering is observed between samples prepared by the FIB milling and FIB-less fabrication methods. All images were taken at a 52° stage tilt.

In general, the resist conditions reported in Table 1 would be adequate for tension testing since the final aspect ratio of the nanopillars at the point of exiting the resist is at least ~1:6. Table 1 does not include specific resist conditions for tension nanopillars since preparing these nanopillars is largely dependent on the geometry of microgrips, which will tense the pillar. In the past, a limited number of groups have reported tension tests on pillars fabricated by FIB milling.[14,31,32] This is because in situ mechanical testing is necessary to properly align the sample with the microgrips. Microgrippers for in situ tension testing are fabricated by FIB machining a standard diamond nanoindenter tip (i.e., Berkovich or cube-corner) in to the desired geometry. Practical use of microgrippers makes it a challenge to prepare nanopillar tension samples with diameters less than ~200 nm. These challenges arise from the large aspect ratios necessary, as well as the minimum size of overplate. For smaller diameter pillars, the resist conditions would have to be altered to extend the gauge length to match that of the microgrips. It was observed that an upper limit exists for the height of smaller diameter nanopillars. For pillars between 75 and 100 nm in diameter, the limit was ~1.2 μm of resist, and for pillars less than 75 nm in diameter the limit was ~750 nm of resist. Beyond these limits, only tapered pillars or

DOI: 10.1021/nl902872w | *Nano Lett.* **XXXX,** *xxx,* 000-000

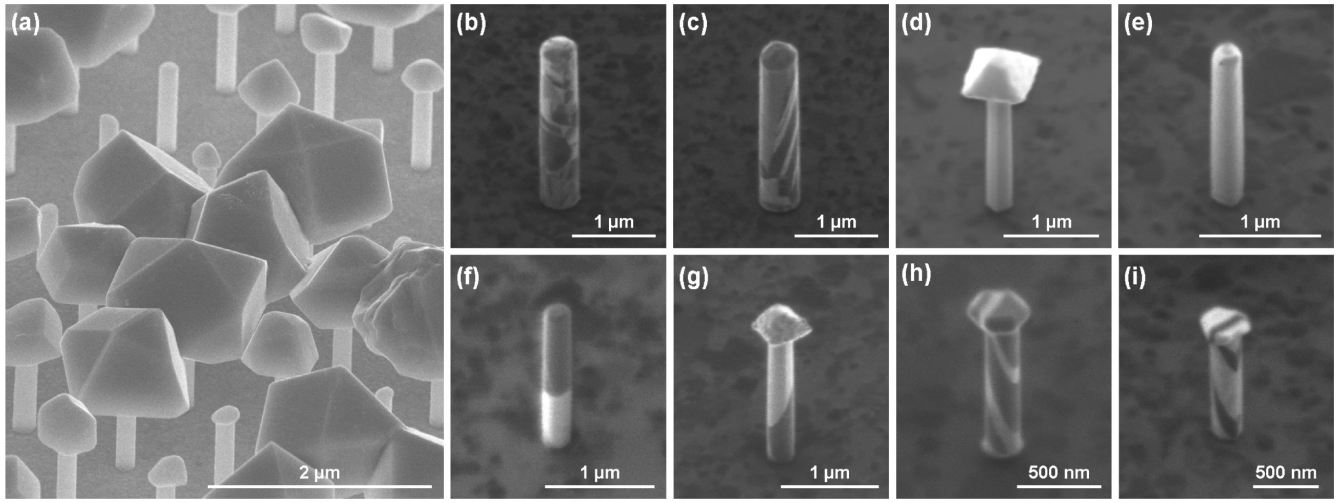

FIGURE 3. SEM image of an array of overplated copper nanopillars (electroplated at 15 mA/cm^2 DC), a diameter of ~175 nm and a gauge length of ~1 μm is shown in (a). FIB images showing grain contrast in 500 nm diameter polycrystalline copper pillars electroplated at 25 mA/cm^2 are shown in (b,c). FIB images of single crystal and bicrystal 250 nm diameter copper pillars electroplated with a 5 s 15 mA/cm^2 forward pulse and 1 s 5 mA/cm^2 reverse pulse are shown in (d,e) and (f,g), respectively. FIB images of 200 nm diameter copper nanopillars electroplated at 15 mA/cm^2 DC showing a unique highly ordered grain structure (most likely nanotwinned) are shown in (h,i). All images were taken at a 52° stage tilt.

pillars with larger than intended diameters were possible to fabricate.

There was no observed limit to the spacing between pillars, although practicality limited this value to roughly 50 μm. It is important to note that the optimal dose value changed significantly when the pillar spacing was increased. Although in most situations clear indicators were fabricated simultaneously with the nanopillars, it was observed that large local indicators had a significant effect on the electroplating for certain conditions. In these instances, only homogeneous pillar arrays were fabricated prior to electroplating, and indicators were reserved for post processing.

Au electroplating was used as a standard to confirm all lithography conditions. This was because the commercial plating solution chemistry, which included extra proprietary additives, was designed for bright finish and high efficiency electroplating. As such, Au electroplating matched closely with calculations made with Faraday's law and was consistent among most plating conditions and all pore sizes. However, as a consequence of the solution chemistry, the microstructure of the Au nanopillars was limited to nanocrystalline, where only relatively small changes in grain size were possible. This was also true with the application of reversed pulse plating. The main reason for limited microstructure control in Au electroplating is the Au sulfite ([Au$(SO_3)_2]^{3-}$) metal salt constituent of the electrolyte, and the polycrystalline nature of the nanopillars is consistent with the previous reported results.[33,34] It is primarily a factor of the relative instability of the Au sulfite salt in solution, which yields liberated Au^+ and SO_3^{2-} ions in solution. The Au^+ ions are believed to undergo a disproportionate reaction, $2Au^+ \rightarrow Au(0) + Au^{3+}$, yielding a precipitate of metallic Au clusters, which are subsequently absorbed on the growing cathode surface and form a polycrystalline nanopillar structure.[33] Another important factor limiting the Au microstructure to nanocrystalline is the inclusion of proprietary plating additives in the commercial solution. Larger grain and single crystal Au plating has been reported in other works by changing the metal salt to Au cyanide ($[Au(CN)_2]^-$) and removing all additives from the solution.[33−35] A similar approach was briefly explored, however initial results showed a chemical incompatibility between the Au cyanide and PMMA (results not reported here). To extend the range of possible microstructures, Cu electroplating was used. The choice to work with Cu stems from the simplistic and inexpensive chemistry available for Cu electroplating. The raw materials to mix the Cu plating solution were readily available, and no extra additives beyond the metal salt and acidic electrolyte were used. With the simple Cu electroplating solution, a much wider range of microstructures were available.

Figure 3 shows the full range of microstructure control available with Cu electroplating. Figure 3a is an SEM image of 175 nm diameter Cu pillars that have been electroplated at 15 mA/cm^2 DC with the plating time purposely increased such as to over plate. These pillars are available for tension testing and have a gauge length of ~1 μm. The faceted nature of the over plates is indicative of large grain deposition. Figure 3 panels b−g are FIB images of Cu pillars plated with various applied currents, both DC and AC. It was observed that current densities above roughly 20 mA/cm^2 DC yield polycrystalline pillars as confirmed by FIB images (Figure 3b,c). It has been shown previously that the grain size scales inversely with the plating overpotential.[35,36] As such, forward current was systematically reduced to yield large grain and single crystal pillars. The lower limit of DC

DOI: 10.1021/nl902872w | *Nano Lett.* **XXXX,** *xxx,* 000-000

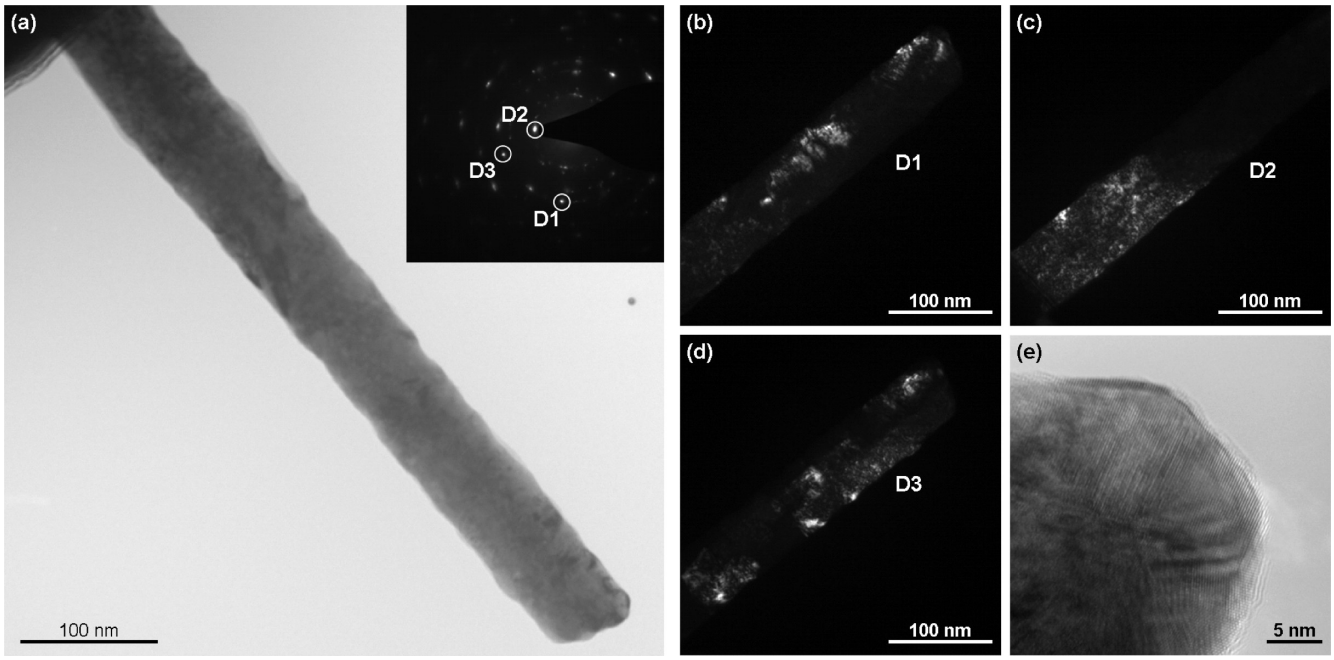

FIGURE 4. Bright field TEM images of an ~50 nm diameter nanocrystalline Au nanopillar electroplated at 3.5 mA/cm^2 DC is shown in (a) with small area electron diffraction pattern taken from the entire pillar displayed in the inset. The sample was prepared using the sacrificial Cr masking method. Corresponding dark field TEM images highlighting specific grains are shown in (b−d). The electron diffraction spots used to highlight specific grains are indicated. High-resolution TEM image of grain boundaries located at the top left corner of the nanopillar are shown in (e).

current density was observed to be 10 mA/cm^2 at which the plating was still successful but with low efficiency. Below 10 mA/cm^2, Cu electroplating was mostly unsuccessful as the supplied current was most likely being used up by the reduction of Cu^{2+} to Cu^{1+} and other side reactions but not in the actual reduction to metallic Cu. At low current densities, FIB images showed a low yield of single crystal pillars (<5% in 250 nm diameter pillars) and a high yield of grains on the order of ~ 100 nm in size. It is believed that DC plating at these low current densities could yield a higher percentage of single crystal pillars in smaller diameter pillars; however this was not further investigated. One important observation to note is that FIB images routinely showed pillars with faceted overplates are not necessarily single crystal and can contain several grains throughout the pillar height before converging into one large grain that then exits the pore.

To further increase the grain size, the plating was conducted with a reverse pulse current (AC) technique. Reverse pulse plating has two advantages over DC plating in terms of large grain microstructure control.[34,37,38] During electroplating, as a reduction potential is applied ions adjacent to the cathode are depleted and a negatively charged layer is formed. When using DC, this layer charges to a finite thickness referred to as the depletion region. This depletion region obstructs the ions from reaching the cathode, making the process diffusion limited. By incorporating reverse pulse electroplating, the reduction potential is periodically turned off, allowing the ions to partially discharge the depletion region, thus lowering the necessary overpotential and increasing the resulting grain size. Also, with AC electroplating, the plating current is temporarily reversed, which introduces a stripping time into the plating cycle. As such, reverse pulse plating selectively dissolves protrusions, defects, or any absorbed impurities off the metal surface, ensuring a more uniform deposition. FIB images of single crystal and bicrystal 250 nm diameter Cu pillars electroplated with a 5 s 15 mA/cm^2 forward pulse and 1 s 5 mA/cm^2 reverse pulse are shown in Figure 3d,e and f,g, respectively. With AC plating, the percentage of single crystal Cu nanopillars increased significantly. For 500 nm diameter Cu pillars electroplated with a 10 mA/cm^2 forward pulse and 3.5 mA/cm^2 reverse pulse, this ratio was calculated to be ~ 60%, with over 250 pillars sampled by FIB imaging. Also observed in samples which were plated with AC conditions were bi- and tri- crystals. One important observation made regarding AC plating is that the reversed pulse segment complicates the fabrication process with respect to future nanomechanical testing. Since the reverse pulse also acts as an electrochemical etch, if the deposition and etch rates are too close the resulting nanopillar often has voids and is inhomogeneous. It was also observed that reverse pulse plating conditions leading to single crystal pillars would also yield pillars which had small voids immediately at the pillar-substrate interface. These voids are believed to appear due to more defects occurring during initial plating before the metal has a chance to fill the pore. As a result of these types of voids, those pillars are not suitable for nanomechanical

DOI: 10.1021/nl902872w | *Nano Lett.* **XXXX,** *xxx,* 000-000

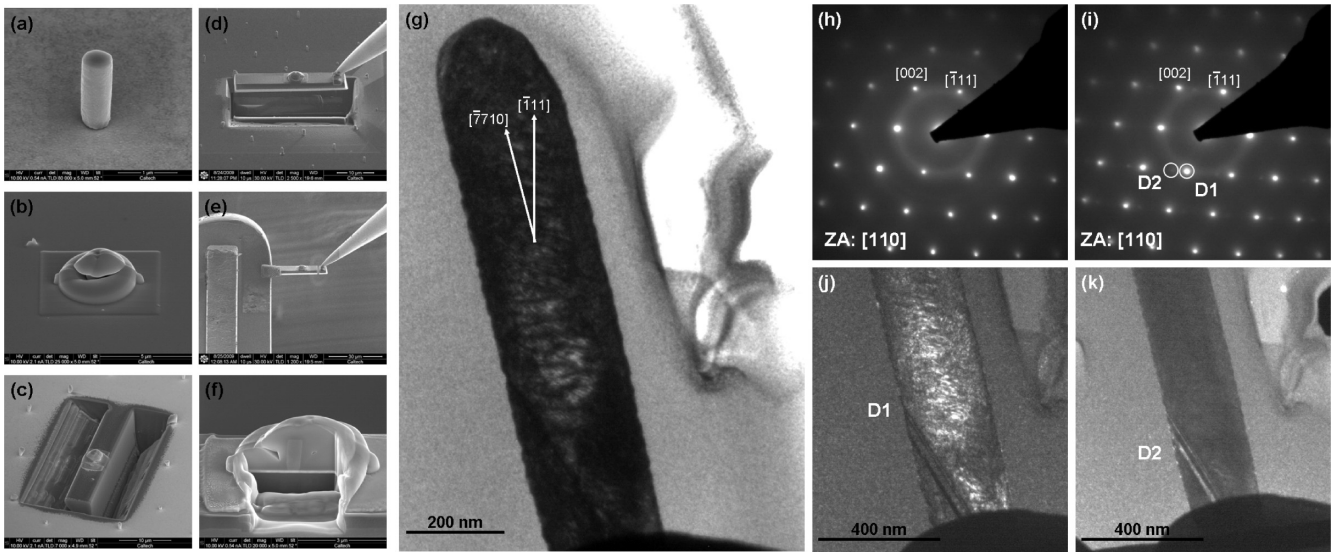

FIGURE 5. A series of images demonstrating the conventional lamella lift out and FIB thinning process for preparation of TEM samples is shown in (a−f). The electroplated pillar (a) is first coated in an ~1 μm protective layer of Pt by local chemical vapor deposition (CVD) via gas injection system (b). An ~30 μm long by 5 μm wide by 5 μm deep lamella (c) is then milled around the pillar in order to isolate it. The lamella is then lifted out via micromanipulator (d) and attached with Pt to a standard Cu TEM lift out grid (e). The micromanipulator is then detached from the lamella (e) and the Pt is thinned on both sides to reveal the pillar (f). A bright field TEM image of an ~250 nm diameter singe crystal Cu nanopillar prepared by the conventional lamella lift out technique is shown in (g). The Cu pillar was electroplated using AC with a 10 mA/cm^2 forward and a 5 mA/cm^2 reverse pulse in a 5s:1s ratio. Small area electron diffraction patterns taken from the top and bottom halves of the pillar are shown in (h) and (i), respectively. These diffraction patterns indicate the nanopillar is a single crystal except for immediately adjacent to the Au seed layer. Corresponding dark field TEM images highlighting specific grains are shown in (j,k). The electron diffraction spots used to generate the dark field TEM images are indicated. The nanopillar axis was determined to be [$\bar{7}$ 7 10], ~10° off of [$\bar{1}$ 1 1].

testing. Figure 3h,i shows FIB images of 200 nm diameter Cu nanopillars electroplated at 15 mA/cm^2 DC showing a unique highly ordered grain structure (most likely nanotwinned). Nanopillars with this type of microstructure were not purposely formed but provide evidence that controlling the formation of highly ordered grain boundaries or twin boundaries in Cu pillars in the future may be possible.

Figure 4 shows TEM analysis of an ~50 nm diameter Au nanopillar electroplated at 3.5 mA/cm^2 DC. The nanopillar was intentionally made overly tall in order to gauge the microstructure through a larger volume. Since the nanopillar was thin enough to be electron transparent, the sacrificial metal masking method was used and the nanopillar was left pristine. The SAED pattern (Figure 4a, inset) was taken from the entire pillar and shows a clear nanocrystalline structure. Several diffraction spots were used in order to generate dark field images highlighting the corresponding grains (Figure 4b−d). Figure 4e is a high resolution TEM image taken at the top left corner of the pillar clearly shows the existence of low angle grain boundaries.

Figure 5a−f shows representative images outlining the conventional lamella lift out TEM sample preparation method. Figure 5g shows a bright field TEM image of a 250 nm diameter Cu nanopillar electroplated with a 10 mA/cm^2 forward pulse and 3.5 mA/cm^2 reverse pulse. The nanopillar was prepared using the conventional Pt coating and FIB thinning technique with the final thickness of ~120 nm. The excessive ion damage is clear, and high resolution imaging was not possible because of it. From the SAED pattern taken from the upper half of the nanopillar (Figure 5h), the microstructure appears to be single crystalline. The SAED pattern taken from the bottom half of the nanopillars (Figure 5i) indicates that there is a second small grain in the area immediately adjacent to the substrate. Dark field TEM images (Figure 5j,k) were generated from the SAED (Figure 5i) and clearly show the existence of one major grain and one small grain boundary near the bottom of the pillar. The nanopillar axis (and loading axis) was determined to be [$\bar{7}$ 7 10], ~10° off of [$\bar{1}$ 1 1].

In conclusion, we have demonstrated an effective method for the FIB-less fabrication of isolated arrays of vertically oriented and virtually taper-free metallic nanopillars suitable for both compression and tension mechanical testing. This technique brings the nanoscale plasticity community closer the desired goal of investigating unique deformation mechanisms operating in nanoscale crystals without the associated effects of Ga^+ induced damage or inhomogeneous stress states in significantly tapered pillars.

AUTHOR INFORMATION

Corresponding Author

* To whom correspondence should be addressed. E-mail: jrgreer@caltech.edu. Tel: (626) 395-4127. Fax: (626) 395-8868.

Acknowledgment. This research is supported by National Science Foundation CAREER GRANT DMR-0748267. The authors thank Dongchan Jang and Andrew Jennings for their

DOI: 10.1021/nl902872w | *Nano Lett.* **XXXX,** *xxx,* 000-000

help with TEM operation and analysis. The authors gratefully acknowledge critical support and infrastructure provided for this work by the Kavli Nanoscience Institute at Caltech.

REFERENCES AND NOTES

(1) Uchic, M. D.; Dimiduk, D. M.; Florando, J. N.; Nix, W. D. *Science* **2004**, *305* (5686), 986–989.
(2) Greer, J. R.; Oliver, W. C.; Nix, W. D. *Acta Mater.* **2005**, *53* (6), 1821–1830.
(3) Dimiduk, D. M.; Uchic, M. D.; Parthasarathy, T. A. *Acta Mater.* **2005**, *53* (15), 4065–4077.
(4) Volkert, C. A.; Lilleodden, E. T. *Philos. Mag.* **2006**, *86* (33), 5567–5579.
(5) Greer, J. R.; Nix, W. D. *Phys. Rev. B: Condens. Matter Mater. Phys.* **2006**, *73* (24), 245410–6.
(6) Rabkin, E.; Nam, H. S.; Srolovitz, D. J. *Acta Mater.* **2007**, *55* (6), 2085–2099.
(7) Tang, H.; Schwarz, K. W.; Espinosa, H. D. *Acta Mater.* **2007**, *55* (5), 1607–1616.
(8) Frick, C. P.; Clark, B. G.; Orso, S.; Schneider, A. S.; Arzt, E. *Mater. Sci. Eng., A* **2008**, *489* (1−2), 319–329.
(9) Shan, Z. W.; Mishra, R. K.; Syed Asif, S. A.; Warren, O. L.; Minor, A. M. *Nat. Mater.* **2008**, *7* (2), 115–119.
(10) Brinckmann, S.; Kim, J.-Y.; Greer, J. R. *Phys. Rev. Lett.* **2008**, *100* (15), 155502–4.
(11) Kim, J.-Y.; Greer, J. R. *Appl. Phys. Lett.* **2008**, *93* (10), 101916–3.
(12) Schneider, A. S.; Clark, B. G.; Frick, C. P.; Gruber, P. A.; Arzt, E. *Mater. Sci. Eng., A* **2009**, *508* (1−2), 241–246.
(13) Deshpande, V. S.; Needleman, A.; Van der Giessen, E. *J. Mech. Phys. Solids* **2005**, *53* (12), 2661–2691.
(14) Kim, J.-Y.; Jang, D.; Greer, J. R. *Scr. Mater.* **2009**, *61* (3), 300–303.
(15) Uchic, M. D.; Dimiduk, D. M. *Mater. Sci. Eng. A* **2005**, *400−401*, 268–278.
(16) Uchic, M. D.; Shade, P. A.; Dimiduk, D. M. *Annu. Rev. Mater. Res.* **2009**, *39* (1), 361–386.
(17) Kiener, D.; Motz, C.; Rester, M.; Jenko, M.; Dehm, G. *Mater. Sci. Eng., A* **2007**, *459* (1−2), 262–272.
(18) Zhang, H.; Schuster, B. E.; Wei, Q.; Ramesh, K. T. *Scr. Mater.* **2006**, *54* (2), 181–186.
(19) Bei, H.; Shim, S.; George, E. P.; Miller, M. K.; Herbert, E. G.; Pharr, G. M. *Scr. Mater.* **2007**, *57* (5), 397–400.
(20) Bei, H.; Shim, S.; Pharr, G. M.; George, E. P. *Acta Mater.* **2008**, *56* (17), 4762–4770.
(21) Martin, C. R. *Science* **1994**, *266* (5193), 1961–1966.
(22) Martin, C. R. *Chem. Mater.* **1996**, *8* (8), 1739–1746.
(23) Hulteen, J. C.; Martin, C. R. *J. Mater. Chem.* **1997**, *7*, 1075–1087.
(24) Schonenberger, C.; van der Zande, B. M. I.; Fokkink, L. G. J.; Henny, M.; Schmid, C.; Kruger, M.; Bachtold, A.; Huber, R.; Birk, H.; Staufer, U. *J. Phys. Chem. B* **1997**, *101* (28), 5497–5505.
(25) Huczko, A. *Appl. Phys. A* **2000**, *70* (4), 365–376.
(26) Kline, T. R.; Tian, M.; Wang, J.; Sen, A.; Chan, M. W. H.; Mallouk, T. E. *Inorg. Chem.* **2006**, *45* (19), 7555–7565.
(27) Richter, G.; Hillerich, K.; Gianola, D. S.; Moñig, R.; Kraft, O.; Volkert, C. A. *Nano Lett.* **2009**, *9* (8), 3048–3052.
(28) Volkert, C. A.; Minor, A. M. *MRS Bull.* **2007**, *32*, 389–399.
(29) Phaneuf, M. W. *Micron* **1999**, *30* (3), 277–288.
(30) Park, C. M.; Bain, J. A. *J. Appl. Phys.* **2002**, *91*, 6830–6832.
(31) Kim, J.-Y.; Greer, J. R. *Acta Mater*, in press.
(32) Kiener, D.; Grosinger, W.; Dehm, G.; Pippan, R. *Acta Mater.* **2008**, *56* (3), 580–592.
(33) Liu, J.; Duan, J. L.; Toimil-Molares, M. E.; Karim, S.; Cornelius, T. W.; Dobrev, D.; Yao, H. J.; Sun, Y. M.; Hou, M. D.; Mo, D.; Wang, Z. G.; Neumann, R. *Nanotechnology* **2006**, *17* (8), 1922–1926.
(34) Dobrev, D.; Vetter, J.; Angert, N.; Neumann, R. *Electrochim. Acta* **2000**, *45* (19), 3117–3125.
(35) Karim, S.; Toimil-Molares, M. E.; Maurer, F.; Miehe, G.; Ensinger, W.; Liu, J.; Cornelius, T. W.; Neumann, R. *Appl. Phys. A* **2006**, *84* (4), 403–407.
(36) Molares, M. E. T.; Buschmann, V.; Dobrev, D.; Neumann, R.; Scholz, R.; Schuchert, I. U.; Vetter, J. *Adv. Mater.* **2001**, *13* (1), 62–65.
(37) Chandrasekar, M. S.; Pushpavanam, M. *Electrochim. Acta* **2008**, *53* (8), 3313–3322.
(38) Dobrev, D.; Vetter, J.; Angert, N.; Neumann, R. *Appl. Phys. A* **1999**, *69* (2), 233–237.

DOI: 10.1021/nl902872w | *Nano Lett.* **XXXX,** *xxx,* 000-000